Distinct and overlapping immunological responses to SARS-CoV-2 and *Mycobacterium tuberculosis* identified by single-cell RNA-seq of co-infected whole blood

Dylan Sheerin[1,2,*], Thanh Kha Phan[1,3], Emily M. Eriksson[2,4], COVID PROFILE Consortium, Anna K Coussens[1,2,5]

[1] Infectious Diseases and Immune Defence Division, Walter and Eliza Hall Institute of Medical Research, VIC 3052, Australia

[2] Department of Medical Biology, The University of Melbourne, VIC 3052, Australia

[3] La Trobe Institute for Molecular Science, Department of Biochemistry and Chemistry, School of Agriculture, Biomedicine and Environment, La Trobe University, Melbourne, Australia

[4] Population Health and Immunity Division, Walter and Eliza Hall Institute of Medical Research, VIC 3052, Australia

[5] Wellcome Centre for Infectious Diseases Research in Africa, Institute of Infectious Disease and Molecular Medicine, Department of Pathology, University of Cape Town, South Africa

*** Correspondence:**

Dylan Sheerin

sheerin.d@wehi.edu.au

Keywords: Tuberculosis, COVID-19, co-infection, single-cell RNA-sequencing, apoptosis.

Abstract

Introduction:

COVID-19 and tuberculosis (TB) exhibit similar symptomatic presentation and clinical parameters. Common underlying immunological mechanisms also highlight potential routes of immunopathogenic interaction between these diseases during co-infection. To explore immunological similarities, differences and interactions, single-cell RNA-seq (scRNA-seq) was performed on whole blood infected with *Mycobacterium tuberculosis* (*Mtb*), SARS-CoV-2, or both pathogens.

Methods:

Whole blood from four healthy adults, were subjected to *ex vivo* infection with *Mtb* and/or SARS-CoV-2 ancestral strain, or were maintained in an uninfected state, for 24 or 96 hours. At each timepoint, for each condition, the four biological replicates were captured, fixed and cryopreserved to be processed for scRNA-seq as a single batch. Following quality control filtering, genotype-based demultiplexing was performed to obtain data from each biological replicate for pseudobulk differential expression analysis.

Results:

Thirteen distinct clusters of cells were identified based on marker gene expression. Profound differences in the proportions of monocytes, T cells and neutrophils were observed between infection conditions and timepoints. The greatest divergence between pathogen responses occurred within myeloid cells at early timepoints of infection. Co-infection had the greatest synergistic effect 24 hours post-infection with 238 immunological pathways uniquely enriched, including IFN-γ and TNF production, whilst by 96 hours post-infection there was a large overlap of 182 shared pathways between *Mtb*, SARS-CoV-2 and co-infection. SARS-CoV-2-only infection resulted in widespread cell death by 96 hours post-infection, while *Mtb*-only and co-infected samples remained enriched for monocyte, T cell and NK cell signatures, sharing negative regulation of extrinsic apoptotic signalling. Distinct from *Mtb*, SARS-Co-V-2 had unique regulating of αβ T cell activation and differentiation at both time points.

Conclusion:

These data provide a high-resolution characterisation of distinct and overlapping immunological responses generated by SARS-CoV-2 and *Mtb* when a single infection or co-infection occurs. This sheds light on the potential effects of novel or existing host-directed therapies that target these pathways, which is particularly crucial for settings where dual presentation is common.

Introduction

The COVID-19 pandemic has had a substantial impact on global progress towards tuberculosis (TB) elimination, primarily through disruptions to TB diagnosis and treatment services [1, 2]. There was a precipitous drop in TB notifications in 2020 and, according to numbers derived from the most recent World Health Organization report, annual deaths from TB have increased between 2019 and 2021 for the first time since 2005 [3], reversing a trend of slow but sustained decline. Beyond impacting TB health services, the Global Tuberculosis Network conducted a prospective multi-country register-based cohort study involving 175 centres across 37 countries, identifying 767 dually diagnosed TB/COVID-19 patients which provided evidence that TB patients suffer worse outcomes when co-infected by COVID-19 [4]. They found that TB/COVID-19 patients experienced 11.1% mortality, compared to 1-2% for COVID-19 alone. A large multi-variate analysis of 3,460,932 patients in South Africa found that current and previous TB increased COVID-19 mortality with adjusted hazard ratios of 2.7 and 1.5, respectively [5]. Despite these epidemiological findings, the immunopathologic interaction between TB and COVID-19 that increases mortality risk remains poorly understood.

The effects of co-infection with *Mycobacterium tuberculosis* (*Mtb*) and SARS-CoV-2 on host immune responses have scarcely been explored in the literature to date. Most published studies have focused on the impact of co-infection on antigen-specific responses to *Mtb* and SARS-CoV-2. These studies have reported that active (clinical) TB limits interferon (IFN)-γ responses to SARS-CoV-2 antigen *in vitro* [6], that COVID-19 patients have lower levels of *Mtb*-specific CD4+ T cells [7] and that "latent" TB infection alters humoral responses to SARS-CoV-2 infection [8] and *vice versa* [9]. A mouse study of *Mtb*/SARS-CoV-2 co-infection demonstrated alteration of the cytokine profile and loss of granulomatous control of *Mtb* in the lung, leading to *Mtb* dissemination [10]. Most recently, immune profiling of TB/COVID-19 co-infected patients revealed significant impairment of antigen-specific responses to the virus and diminished *in vitro Mtb*-specific responses in co-infected patients compared with those with TB-only [11]. Taken together, these data demonstrate an alteration of the ability of the host to respond to and control *Mtb* and/or SARS-CoV-2 in the event of co-infection, prompting further exploration of the underlying immunological pathways.

We previously performed a patient-level meta-analysis of published COVID-19 immune cell signatures on publicly available TB RNA-seq datasets to identify potential immunological hotspots that could exacerbate disease, identifying neutrophil, monocyte, lung macrophage subpopulations,

interferon and complement signalling particularly shared between severe COVID-19 and active and subclinical TB [12]. However, a detailed exploration of the responses to genuine co-infection in humans was lacking. We therefore elected to study these responses in human whole blood at single-cell (sc) resolution by subjecting blood samples from four healthy adults to *ex vivo* infection with *Mtb* and/or SARS-CoV-2 for subsequent scRNA-seq at 24 and 96 hours post-infection (p.i.). By defining longitudinal gene expression changes induced by each infectious agent, relative to uninfected samples, and comparing these responses with co-infected samples, we were able to discern unique aspects of the immune response to each pathogen and which responses are exacerbated by co-infection. The present study provides the most comprehensive overview of the immunological interaction between these two globally significant pathogens to date.

Materials and Methods

Mycobacterium tuberculosis Single Cell Stock Generation

T25 flasks (Sigma Aldrich) containing 10 mL 7H9 (Difco™ Middlebrook 7H9 broth, Becton Dickinson)/ADC (Becton Dickinson) media containing 0.05% Tween-80 (Sigma-Aldrich) were inoculated with 500 µL frozen aliquots of the *Mtb* lineage 4 laboratory strain H37Rv. Flasks were incubated at 37°C for 10 days. Cultures were transferred to 50 mL Falcon tubes (Fisher Scientific) using a serological pipette on day 10 during exponential growth phase. One millilitre of culture was transferred to a 500 mL flask containing 100 mL 7H9/ADC media without Tween-80 and incubated at 37°C for a further 10 days, swirling intermittently after day four. On day 10, 50 mL aliquots were centrifuged at 3000 x *g* for 5 minutes at room temperature. Supernatants were removed and ~10 glass beads (2–3 mm, Sigma-Aldrich) were added to the pellets and shaken vigorously for 1 minute. Six mL Dulbecco's phosphate-buffered saline (DPBS, ThermoFisher) was added to each tube and mixed by inversion before allowing clumps to decant for 10 minutes. The upper 5 mL was decanted into a separate tube and centrifuged at 260 x *g* for 10 minutes at room temperature. The upper 4.5 mL of supernatant was transferred into a new tube containing 0.5 mL 50% glycerol (ThermoFisher) and aliquots stored at -80°C. One frozen aliquot was serially diluted in quadruplicate for plating on three-sector 7H10 (Difco™ Middlebrook 7H10 agar, Becton Dickinson)/ADC plates for colony forming unit (CFU) determination, incubated at 37°C and counted after 10, 14 and 21 days.

SARS-CoV-2 Stock Preparation

Vero (CCL-81, ATCC) cells were cultured in T150 flasks in Dulbecco's Modified Eagle Medium (DMEM + 1 g/L D-glucose, L-glutamine and 110 mg/L sodium pyruvate, ThermoFisher) + 10% heat-inactivated foetal bovine serum (FBS, Sigma-Aldrich) until confluent. Media was removed and adherent cells were washed twice with DPBS before replacing with 10 mL serum-free DMEM. A single 1 mL vial of VIC001 (24/03/21) SARS-CoV-2 stock (1 x 10^6 tissue culture infectious dose 50 [TCID50]/mL, obtained from The Peter Doherty Institute for Infection and Immunity, Melbourne, Australia) was thawed. Infection media was made up by adding VIC001 stock to serum-free DMEM to achieve an MOI of 0.01 (1 x 10^5 TCID50 for ~1 x 10^7 cells) and adding TPCK-treated trypsin (ThermoFisher) to a final concentration of 1 µg/mL. 2.5 mL of infection media was added to the Vero cells in the flask after removing the serum-free media and incubated at 37°C with 5% CO_2 for 30 minutes. 20 mL of serum-free DMEM + TPCK trypsin was added to the flask and incubated at 37°C with 5% CO_2 for 48 hours or until sufficient cytopathic effect was observed under the microscope.

Infection media was removed from the T125 flask, transferred to a 50 mL Falcon tube and centrifuged at 3000 x *g* for 10 mins to pellet the debris. Supernatant was transferred to a separate 50 mL Falcon tube, taking care to avoid the pellet, and then aliquoted into 1 mL Nunc® CryoTubes® to be stored at -80°C. Vero cells were seeded in flat-bottomed 96-well plates (ThermoFisher) at a density of 1 x 10^4 cells/well and incubated at 37°C with 5% CO_2 overnight to achieve confluency. Media was removed from wells and cells were washed twice with DPBS before replacing with 125 µL of DMEM + TPCK trypsin [13]. One aliquot was used to measure TCID50 of the stock by diluting in 1:7 serial dilutions five times with six replicates in serum-free DMEM + TPCK trypsin in a round-bottom 96-well plate (ThermoFisher). Twenty-five microlitres of each dilution was transferred to the appropriate well of the 96-well Vero plate and incubated for four days at 37°C with 5% CO_2. TCID50 values were calculated by scoring wells (positive or negative) for cytopathic effect (CPE) on day four, using the Spearman and Kärber method [14].

Blood Collection

Acquisition of human blood samples and immunological investigations were approved by the Human Research Ethics Committee at the Walter and Eliza Hall Institute (WEHI HREC #18_09LR and #20/08) and Melbourne Health (RMH69108) as part of the COVID PROFILE study [15]. Sample and study data were collected and managed using REDCap [16, 17] electronic data capture tools hosted by Clinical Discovery and Translation, WEHI, Parkville, Victoria, Australia. All subjects provided written informed consent to participate in this study, in accordance with the Declaration of Helsinki. Blood collected in sodium heparin tubes from four donors (2 males, 2 female) were divided into eight 1 mL aliquots (approximately 5 x 10^6 cells/mL) for two timepoints (24 and 96 hours) and four conditions – uninfected, *Mtb*-infected, SARS-infected and co-infected.

Blood Infections

Mtb-only blood samples were infected with *Mtb* at 4 x 10^4 CFU in a volume of RPMI equivalent to the volume of blood. For SARS-CoV-2-only, blood samples were pelleted at 300 x *g* for 5 minutes, plasma were transferred to a clean 15 mL tube (Eppendorf), 5 x 10^6 viral particles of SARS-CoV-2 (MOI 1) was added to a volume of RPMI + TPCK trypsin equivalent to the volume of supernatant removed and incubated at 37°C for 30 minutes. After incubation, plasma was replaced and RPMI equivalent to the starting volume of blood added. For co-infected samples, RPMI was made up with *Mtb* at 4 x 10^4 CFU/mL before adding. An equivalent volume of RPMI as also added to uninfected samples. All samples were placed on an orbital rotator in a 37°C incubator with 5% CO_2 for 24 or 96 hours.

Single-cell RNA-sequencing

Cells were harvested at the appropriate timepoint by pelleting at 300 x *g* for 5 minutes, removing supernatant, resuspending pellets in an appropriate volume of red blood cell lysis solution (0.15 M NH_4Cl, 0.01 M $KHCO_3$, 0.1mM EDTA), incubating for 10 minutes and repeating with an RPMI wash. Cells in a 1 mL RPMI suspension were counted using a Countess automated cell counter (ThermoFisher). Equal numbers of cells from each of the four donors were combined for each condition and a total of eight HIVE™ (Honeycomb Biotechnologies) cell capture devices, one for each condition, were loaded with 30,000 total cells according to manufacturer's instructions to fix cells and sterilise both pathogens. To confirm SARS-CoV-2 inactivation, Honeycomb™ fixative was mixed 1:1 with SARS-CoV-2 RPMI infection media and diluted out to 1:100 final concentration before putting on a Vero cell monolayer. TCID50 assay was performed as detailed above and compared against Vero cells incubated with SARS-CoV-2 RPMI infection media and uninfected Vero cells (Supplementary Figure 1). To confirm *Mtb* inactivation, Honeycomb™ fixative was mixed 1:1 with 2 x 10^4 CFU of *Mtb* in 7H9/ADC growth media, to a total volume of 1 mL, and 200 µL was dispensed into triplicate wells of a flat-bottomed 96-well plate (ThermoFisher). Growth media was used as a negative control and growth media + *Mtb* was used as a positive control. The 96-well plate was incubated at 37°C for 14 days before adding alamarBlue (ThermoFisher), at 10% of sample volume to each well, and incubating overnight. Fluorescence was measured at 555-590 nm the next day to determine *Mtb* viability (Supplementary Figure 2). Loaded HIVEs were stored at -80°C until ready for further processing. All eight HIVE™ devices were processed to cDNA in a single batch according to manufacturer's instructions (v1 revision A). Final library concentrations were measured using a KAPA Library Quantification Kit (KAPA Biosystems) and profiled on a Tapestation (Agilent) before pooling at equimolar concentrations for Illumina NextSeq 2000 (Illumina) sequencing with custom primers (Honeycomb Biotechnologies).

Data Analysis

The bespoke HIVE™ BeeNet™ pipeline (v1.1, Honeycomb Biotechnologies, https://honeycombbio.zendesk.com/hc/en-us/articles/4408694864283-BeeNet-v1-1-X-Software-Guide) was used to process the raw data into count matrices. First of all, the *make-ref* function was used to generate a human reference genome index from the GRCh38 Homo sapiens reference genome fasta and annotation gtf files (https://ftp.ensembl.org/pub/release-109/fasta/homo_sapiens/). Fastq files were aligned to this index using the BeeNet™ *align* function and transcript count matrices were obtained for each sample. To demultiplex the four donors combined in each sample, cellsnp-lite [18] was used to pileup expressed alleles in the data and vireo [19] was subsequently

used to assign cells to donors. Donor ID probabilities obtained from these algorithms were used as metadata for downstream analyses requiring biological replicates.

The Seurat pipeline was applied to count matrices for downstream analyses (https://satijalab.org/seurat/). A Seurat object was created for each of the eight samples, combined into a merged Seurat list and subjected to quality control filtration. Features with fewer than 500 genes and 500 unique transcripts were removed and a threshold of <15% mitochondrial reads was used to filter down to the final total cell numbers per sample for analysis. Each object in the merged list was subjected to log normalization and variable feature identification, using variance stabilising transformation and 2000 features [20]. Objects were integrated by selecting integration features, finding integration anchors based on these features and using the integration anchors as input for the Seurat *IntegrateData* function [21]. The resultant integrated data object was scaled and subjected to principal component (PC) analysis before graph-based K-nearest neighbour cluster identification was performed. Non-linear dimensionality reduction was performed using uniform manifold approximation and projection (UMAP) on the first 10 dimensions.

Cell type annotation was conducted using SingleR and the Human Primary Cell Atlas Data obtained via the celldex package [22]. Cluster markers were identified by running the Seurat *FindAllMarkers* function using the default Wilcoxon Rank-Sum test to define differentially expressed genes (DEG). Gene ontology (GO) and Reactome pathway enrichment analysis were performed using the identified markers and by invoking the org.Hs.eg.db, AnnotationDbi and clusterProfiler packages [23]. A stringent *p*-value cut-off of 0.001 was applied after Benjamini Hochberg adjustment for multiple testing.

To perform pseudobulk differential expression analysis, the Seurat object was first converted to a SingleCellExperiment class. Cluster counts and metadata for each donor were then aggregated and extracted and used to create DESeq2 [24] objects. Counts were transformed for clustering analyses (Supplementary Figure 3) before running the *DESeq* function. Log_2 fold-change (LFC) shrinkage and Wald tests were performed for each contrast of interest to obtain results tables for all genes. Those with false-discovery rate (FDR)-adjusted *p*-values <0.05 and LFC values >0.58 were deemed significant (Supplementary Table 1–6). GO analyses of pseudobulk data were performed using the clusterProfiler [23] and tmod [25] packages.

Results

Pathogen-specific changes in immune cell proportions recovered from peripheral blood emerge over the course of infection

Following acquisition of scRNA-seq data, quality control analysis was first performed on the raw scRNA-seq data acquired from each individual sample from our 8 biological conditions: uninfected, *Mtb*-only, SARS-CoV-2-only (SARS-only) and co-infection, at 2 time points. Each sample was then filtered to exclude cells with <500 genes/transcripts and >15% of reads mapping to mitochondrial genes (indicative of dying cells). This resulted in total cell counts ranging from 367–3,894 (median 2,340), and an overall total of 18,990 cells. Normalisation and feature selection were performed prior to data integration, and dimensionality reduction was subsequently performed on the integrated data. *ANPEP*, a gene which encodes alanine aminopeptidase, a receptor known to facilitate the binding and entry of coronaviruses, was the top gene contributing to the first principal component (PC1) of the data (Figure 1A). In addition to multiple genes involved in macrophage and endothelial cell adhesion and migration, *RAB31*, which encodes a GTPase implicated in the maturation of phagosomes which engulf *Mtb*, was among the top 10 genes contributing to PC1 (Figure 1A).

Fourteen clusters were identified based on underlying gene expression differences in the integrated data which were broadly categorised by applying cell type annotation into eight distinct immune cell populations (Figure 1B). The integrated data were then split by infection condition at each time point to begin comparing cell clusters (Figure 1C). Yields for each cell type were similar overall between 24 hours and 96 hours p.i. for the uninfected and *Mtb*-only samples, but there was fewer cells recovered in the SARS-only and co-infected samples at 96 h p.i (Figure 1C, Table 1). SARS-only had the lowest number of cells recovered at this time point, with just 367 remaining after quality filtering (Table 1). Neutrophils made up a greater proportion of the SARS-only and co-infected samples at 24 hours p.i. (68% and 52% of recovered cells, respectively) compared to uninfected and *Mtb*-only (27% and 23%, respectively), with SARS-only having the lowest proportions of CD4+ T cells, CD8+ T cells, B cells and NK cells of all four conditions (Supplementary Figure 4). This represented a 17% and 12% increase for each of the two identified neutrophil populations in the SARS-only samples, relative to the uninfected samples, while the second population accounted for a 33% increase in the co-infected samples (Figure 1D). At 96 hours p.i., several immune cell populations were more abundant in the *Mtb*-only samples relative to the uninfected samples (Figure 1D, Table 1), including B cells (88%), LPS-responding neutrophils

(95%), NK cells (35%) and CD4+ T cells (33%). With the exception of B cells, the later 3 cell types were also all higher in the co-infected samples compared with the SARS-only samples at this timepoint, suggesting *Mtb* may be sustaining their viability.

Table 1. Cell counts for each of the remaining cells belonging to each annotated immune cell populations after quality control filtration for each infection condition and timepoint.

	24 hours post-infection				96 hours post-infection			
Cell type	**Uninfected**	***Mtb*-only**	**SARS-only**	**Co-infected**	**Uninfected**	***Mtb*-only**	**SARS-only**	**Co-infected**
Monocytes	2158	1106	904	740	2601	1464	190	588
Neutrophils (GM-CSF/ IFN-γ)	451	158	979	318	317	92	38	60
Neutrophils (LPS)	618	297	1313	820	93	181	17	56
CD8+ T cells	304	145	70	87	339	275	47	81
CD4+ T cells	247	176	47	138	259	344	46	143
NK cells	67	63	17	55	55	74	15	42
HSC (G-CSF)	34	24	48	28	29	34	9	14
B cells	15	12	2	15	8	15	5	3
Total (18,990)	**3894**	**1981**	**3380**	**2201**	**3701**	**2479**	**367**	**957**

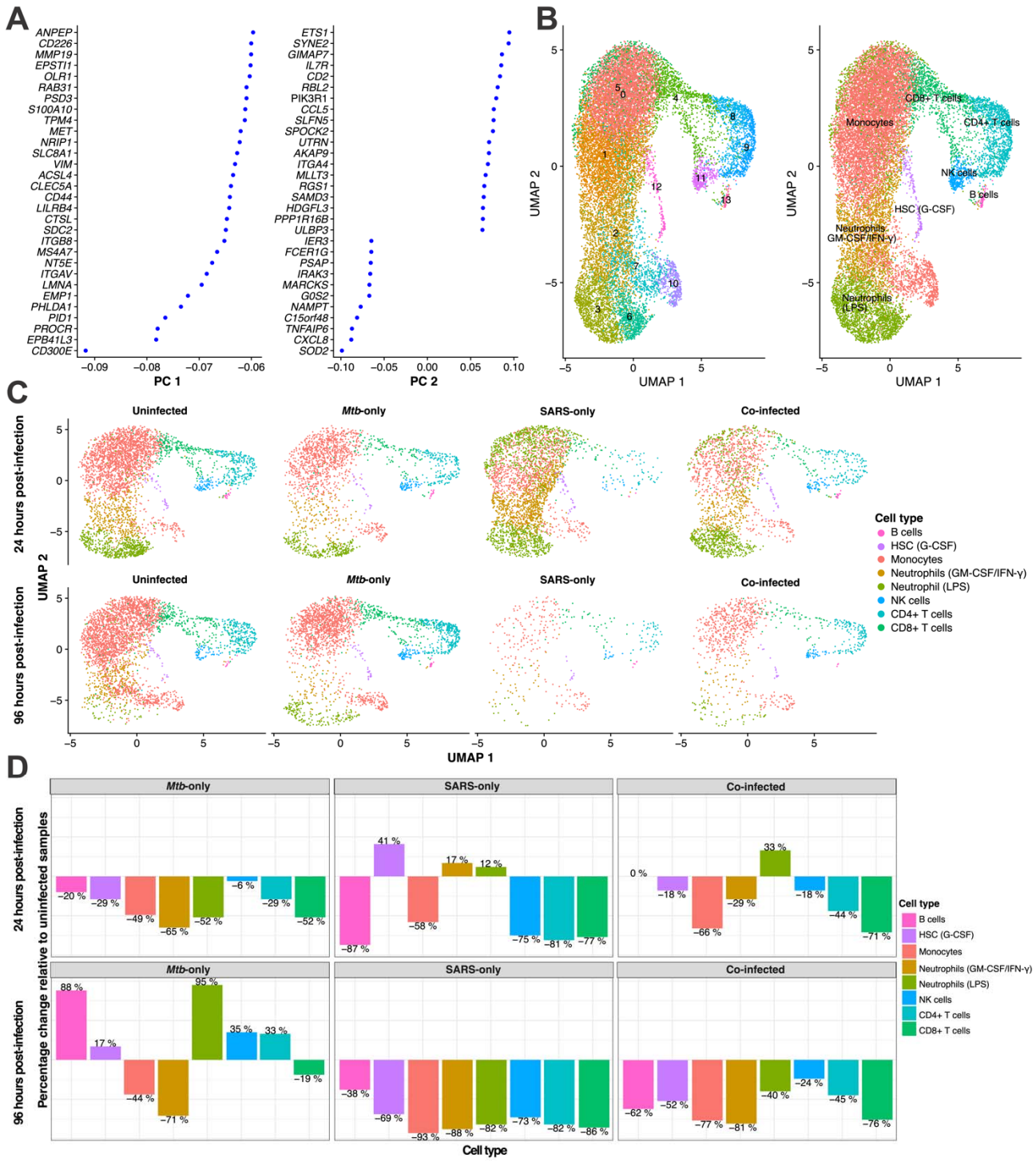

Figure 1. Global changes to the transcriptome of human whole blood in response to single or dual *Mtb*/SARS-CoV-2 infection. A. The top 30 genes contributing to the first two principal components (PC) identified by performing dimensionality reduction on the integrated scRNA-seq from all eight samples. **B.** Uniform manifold approximation and projection (UMAP) plot depicting clustering of cells across all eight samples identified by shared nearest neighbour modularity optimisation. Clusters are here grouped according to either the 14 identified clusters (0-13, left) or one of eight distinct immune cell type annotations (right). **C.** UMAP plots depicting clustering of cells across these eight samples separated for each condition (x-axis) and timepoint (y-axis) and

coloured by the eight distinct immune cell type annotations. **D.** Bar plots depicting the percentage change in cell count for each of the annotated cell clusters relative to the uninfected samples at the same timepoint, for each infection condition.

Distinct immunological pathway enrichment highlights cells responding to infection

For the 14 identified clusters, covering the eight distinct immune cell populations, GO and Reactome biological process (BP) pathway enrichment analyses were performed to determine whether they were associated with distinct immune functions. Pathways were filtered to display the most salient terms in Figure 2, with the full lists provided in Supplementary Tables 7–8. Clusters 1, 2, 5 and 7 were associated with the greatest number of significantly enriched pathways. While clusters 2 and 5 are both predicted to be neutrophil populations, cluster 2 is characterised by its response to GM-CSF and IFN-γ, whereas cluster 5 is characterised by its greater enrichment of response to LPS. Cluster 5 was found predominantly in the SARS-only and co-infected samples at 24 hours p.i. (Figure 1C); clusters 3 and 6 were also classified as LPS-responding neutrophils but were not associated with statistically significant enrichment of these pathways at this timepoint. The GM-CSF/IFN-γ-responding neutrophils were associated with the largest number of significantly enriched GO pathways and, as predicted by their annotation, they were defined by response to IFN-γ, production of TNF, cytokine signalling, endocytosis and neutrophil migration (Figure 2A). Furthermore, this cluster was significantly enriched for Reactome pathways denoting IFN-α/β signalling, Fc-γ receptor-dependent phagocytosis and interleukin signalling (Figure 2B). The genes implicated in the enrichment of the interleukin signalling term included pro-inflammatory mediators and chemokines *SOD2*, *IRAK1*, *PTAFR*, *IL1B*, *SYK*, *TNFRSF1B*, *CXCL2*, *CSF3R*, *HCK*, *CCL3L1*, *GRB2*, *CCL20*, *CDKN1A*, *CXCL1*, *STAT1*, *CCR1*, *MAP3K8*, *IL1R1*, *CXCL10*, *VEGFA*, *IL1A* and *PTPN12*. Conversely, the LPS-responding neutrophils were exclusively significantly enriched for GO pathways indicating metal ion sequestration and homeostasis (*LCN2*, *FTL*, *TFR2*, *LTF*, *PRNP*, *SLC39A7*, *SLC11A1*, *S100A8* and *S100A9*), regulation of leukocyte cell-cell adhesion, response to chemokine (also confirmed by Reactome pathway analysis, Figure 2B), and negative regulation of cell adhesion and IFN-γ production (Figure 2A). Clusters 1, 7 and 10 represent subsets of monocytes, with clusters 1 and 7 both enriched for antigen processing and presentation via MHC class II. Cluster 7 is exclusively enriched for peptide antigen assembly with MHC class II protein complex, whilst Cluster 1 is exclusively enriched for myeloid leukocyte migration, superoxide anion generation and membrane lipid catabolic process and Cluster 10 is exclusively enriched for foam cell differentiation (*ITGAV*, *PPARG*, *MSR1*, *NR1H3*, *IL18*, *ITGB3* and *LPL*).

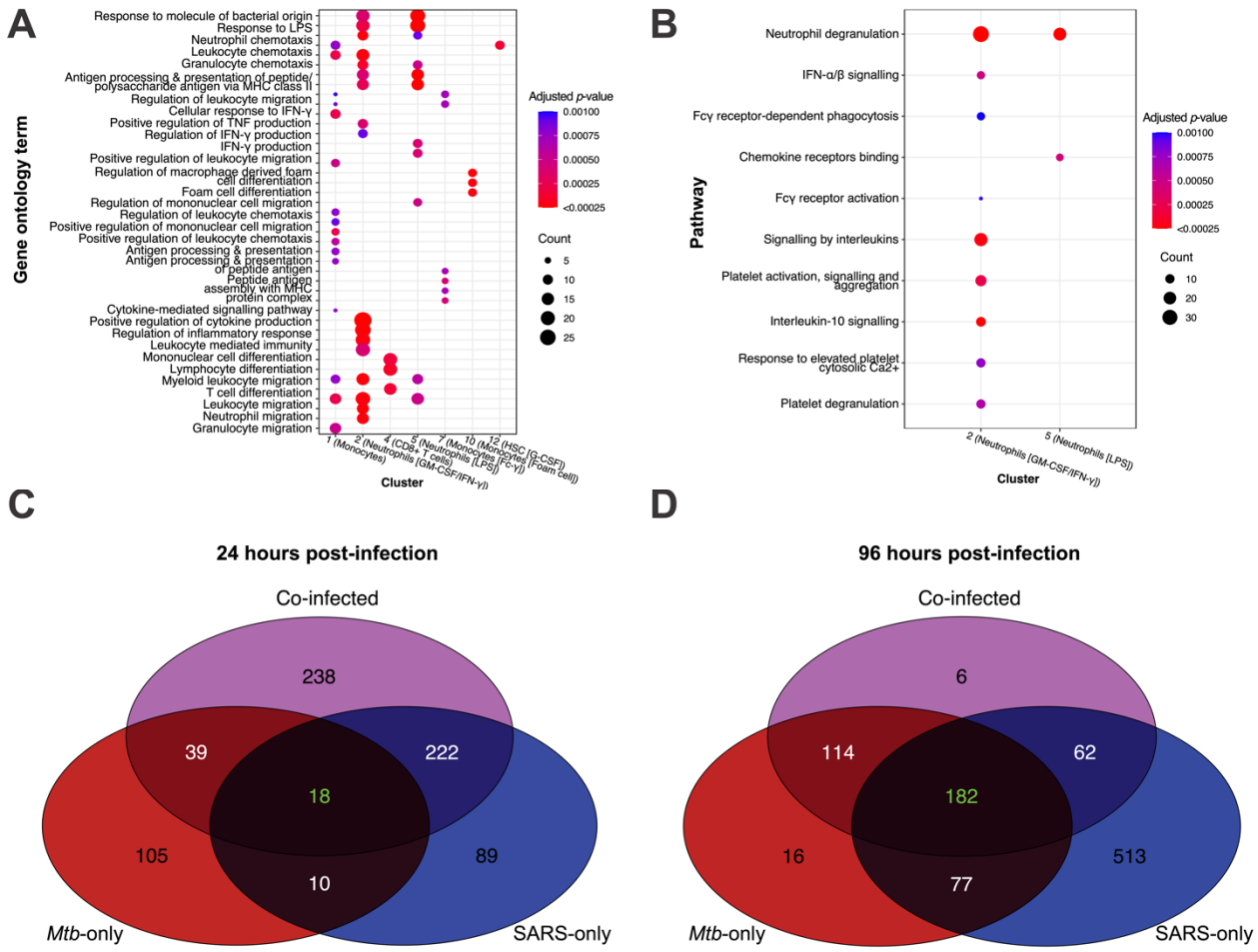

Figure 2. Substantial immune pathway enrichment underpins identified cell clusters and exhibits greatest divergence between conditions at 24 hours post-infection. 14 identified clusters of cells were consolidated to eight immune cell populations based on cluster annotation. Cell marker genes were identified by performing a Wilcoxon Rank Sum tests between each of the eight annotated immune cell populations, irrespective of sample. These differentially expressed gene (DEG) lists were then subjected to a biological process (BP) enrichment analysis using **A.** gene ontology (GO) or **B.** Reactome pathway annotation. False discovery rate-adjusted *p*-values are representing by the shading of data points, while the size corresponds to the number of significant genes implicated in that pathway. A pseudobulk analysis was performed between infection conditions at each timepoint by combining cells in each condition and using standard differential expression (DE) methods, with each of the four composite donor IDs as replicates. Significant DEGs were then subjected to a BP GO enrichment analysis and the overlap in GO terms was assessed by venn diagram at **C.** 24 hours and **D.** 96 hours post-infection.

Co-infection demonstrates synergistic global immune pathway enrichment at 24 hours, and greater shared pathways by 96 hours, of infection

To ascertain whether differences in immunological pathway enrichment existed between each infection condition, compared to uninfected, a pseudobulk analysis was performed using donor IDs as biological replicates and performing differential expression analyses across all cell types between conditions. A similar GO and Reactome pathway enrichment analysis (Figure 2A-B, Supplementary Table 9-10) was then performed on the significant genes identified (Supplementary Table 1–6). Assessing the unique and overlapping significantly enriched terms revealed distinct aspects of the immune response invoked by each infection condition, at both time points. At 24 hour p.i SARS-only and coinfection shared the greatest overlap in terms (222), compared to only 39 commonly enriched terms between *Mtb*-only and co-infection however, this pattern was switched at 96 hours p.i. with *Mtb*-only and co-infection sharing 114 terms compared to only 62 shared terms between SARS-only and co-infection. This demonstrates that the influence of each pathogen on the transcriptome changes during the course of co-infection, with the influence of *Mtb* increasing during co-infection as it replicates over time.

Looking at terms unique to each pathogen, 105 were enriched for *Mtb*-only and 89 for SARS-only at 24 hours p.i.. Of the biologically relevant GO terms for this analysis, certain generic immune cell activation pathways and immune effector processes were uniquely enriched in *Mtb*-only infected cells at 24 hours p.i., while B cell activation (GO:0042113), Fc receptor and STAT signalling (GO:0038094, GO:0097696), and several other cell signalling/response to cytokine GO terms were unique to SARS-only infection (Supplementary Table 9). Amongst the 222 enriched terms shared between SARS-only and co-infection at 24 hours p.i. were αβ T cell activation and differentiation (GO:0046631, GO:0046632), antimicrobial humoral immune response mediated by antimicrobial peptide (GO:0061844), negative regulation of extrinsic apoptotic signalling (GO:2001237), extracellular matrix disassembly (GO:0022617), negative regulation of cell-cell adhesion (GO:0022408), positive regulation of phagocytosis (GO:0050766), regulation of coagulation (GO:0050818), IFN-γ signalling (GO:0034341), IL-1/2/6 production (GO:0032612, GO:0032623, GO:0032635), leukocyte/lymphocyte proliferation (GO:0070661, GO:0046651) and migration (GO:0050900, GO:0072676), antigen processing and presentation (GO:0019882) and defence response to virus (GO:0051607). Amongst, the 39 terms shared between *Mtb*-only and co-infection at 24 hours p.i. included seven related to cell cycle/division, and others relating to endothelial cell migration (GO:0043542) and regulation of cell differentiation (GO:0045595, Supplementary Table 9).

By 96 hour p.i. *Mtb*-only and co-infection were enriched for 114 shared terms including negative regulation of extrinsic apoptotic signalling (GO:2001240) and TNF production (GO:0010804),

antigen processing and presentation via MHC class II (GO:0002495), cell death in response to oxidative stress (GO:0036473), iron homeostasis (GO:0006879), endothelial cell migration and proliferation (GO:0043542, GO:0001935), LPS metabolic process (GO:0008653), and reactive nitrogen species (GO:2001057); while SARS-only and co-infection shared 62 terms including myeloid cell differentiation (GO:0030099), pattern recognition receptor/TLR signalling (GO:0002221, GO:0002224) and positive regulation of reactive oxygen species metabolic process (GO:2000379). At 96 hours p.i *Mtb* infection had only 16 unique terms (of its total 389), including WNT signalling (GO:0016055), whereas SARS-only infection had the largest number of enriched terms and the largest number of unique terms at this time (513 of 834 terms, ~62%, Figure 2D). However, the unique terms included many variations on terms collectively shared between all three infection conditions at this timepoint (described below) with the additional enrichment of αβ T cell activation and differentiation (GO:0046631, GO:0046632), ephrin receptor signalling pathway (GO:0048013), Fc epsilon receptor signalling (GO:0038095), granulocyte migration (GO:0097530), intrinsic apoptotic signalling (GO:0097193), macrophage activation (GO:0042116), IL-2/6/8 production (GO:0032623, GO:0032635, GO:0032637), monocyte chemotaxis (GO:0002548), and response to IL-1 (GO:0071347) and type I IFN (GO:0034340); many of these terms being shared between SARS-only and co-infection at 24 hours p.i. Thus, over the time course of infection very few of these pathways were unique to SARS-CoV-2 with the majority regulated at one time by both pathogens, just the kinetics varying. Finding the largest enrichment of pathways in the SARS-only infected cells at 96 hours p.i. with this also being the condition with smallest cell recovery, suggests the dominance of the immune response to SARS infection in the absence of *Mtb* co-infection, with the increased cell recovery for co-infected samples perhaps due to survival signals induced by *Mtb* infection.

Next, when comparing how the pathogens interact during co-infection, first comparing the similarity between all three conditions (i.e. terms shared with no synergistic effect of co-infection) there were only 18 collectively shared terms at 24 hour p.i (Figure 2C), all of which were related to generic biological functions and not specific to infection (Supplementary Table 9). By contrast, co-infection was associated with 238 uniquely enriched terms the largest number across all infection conditions at 24 hours p.i., indicating the synergistic nature of the response to dual infection, identifying terms not induced by either pathogen alone (Figure 2C); uniquely enriched terms included IFN-γ and TNF production (GO:0034341, GO:0034612), lymphocyte activation/differentiation (GO:0046649, GO:0030098), NK cell-mediated immunity (GO:0002228), T cell signalling (GO:0050852) and positive regulation of viral process (GO:0048525). However by 96 hours p.i. only 6 terms where unique to the co-infection group, indicating limited synergistic

pathway enrichment, but there were now 182 terms common between *Mtb*-only, SARS-only and co-infection (Figure 2D); these included antimicrobial humoral response, B cell activation, T cell differentiation, reactive oxygen species processes, regulation of viral life cycle, lipoprotein metabolic process, tissue remodeling and receptor mediated endocytosis (Supplementary Table 10). Together this shows that *Mtb* and SARS-CoV-2 share a large overlap in immune pathway enrichment which they each induce during infection with early synergism during co-infection.

Finally, at 24 hours p.i there were an additional 10 terms commonly enriched in *Mtb*-only and SARS-only, not shared by co-infection, increasing to 77 commonly enriched terms for the two mono-infections at 96 hours p.i. These terms would be independently but not synergistically regulated by each pathogen, and may include pathways were each pathogen has opposing effects such that during co-infection pathway enrichment is lost.

Specific differences between infection conditions are most apparent in innate populations and within the first 24 hours of infection

To further examine specific differences and overlapping gene expression between the infection conditions a second pseudobulk analysis was performed, this time at the level of annotated immune cells. For each of the infection conditions, immune cell populations were contrasted against the equivalent cell type in the uninfected group for that timepoint. No significant DEGs were detected in the B cell or haemopoietic stem cell (G-CSF) populations, likely due to the small numbers of cells of this type per donor/condition. The LPS-responding neutrophils at 24 hours p.i. were associated with the greatest number of DEGs across all groups (1,470), with the majority of these induced by co-infection and SARS-only (1,260 total, 434 unique, Supplementary Figure 5), followed next by monocytes (772 total DEG) and neutrophils (GMCSF) (626 total DEG) at 24 hours p.i. For all cell types with associated differential expression, there were very few DEGs uniquely associated with *Mtb*-only at 24 hours p.i., at which timepoint SARS-only and co-infection induced the greatest DE, while *Mtb*-only and co-infection induced the greatest DE at 96 hours p.i. when SARS-only induced the least DE of all three conditions (Supplementary Figure 5). This supports a more acute unique transcriptional perturbation associated with SARS-CoV-2 at the initial stages of infection, while *Mtb* induces a response shared by SARS-CoV-2 and co-infection early on which becomes more distinct from SARS-CoV-2 at the later time point after infection is established. The co-infected samples remained highly transcriptionally active throughout both timepoints due to the presence and synergism of both pathogens.

Clustering by DEGs identified for monocyte and neutrophil populations generated the cleanest sample clustering by infection condition and timepoint (Figure 3A compared with NK, CD4+ and CD8+ T cell populations (Supplementary Figure 6). At 24hr p.i monocyte expression clustered together for *Mtb*-only and co-infection, whilst co-infection had the most unique monocyte expression at 96 hours p.i., with *Mtb*-only and SARS-only clustering more closely together at this later timepoint. Conversely, patterns of neutrophil gene expression clustering were most distinct at 24 hours p.i at which time GM-CSF neutrophils shared a similar expression pattern between *Mtb*-only and SARS-only infections, whilst LPS neutrophils clustered together for co-infection and SARS-only.

Finally, the functional enrichment underlying these similarities and differences was assessed at each timepoint. At 24 hours p.i., the majority of enriched pathways were shared by SARS-only and co-infected samples and related to type I IFN responses from monocytes, neutrophils and CD4+ and CD8+ T cells, cell activation (IL-15, IL-23, TNF) of monocytes and neutrophils (GM-CSF, RIG-I like receptor signalling of monocytes, neutrophils (GM-CSF) and CD4+ T cells and viral sensing & immunity; IRF2 targets networks for monocytes and both neutrophil subsets (Figure 3B, Supplementary Table 11). By comparison, there less cell-specific pathway enrichment at 96 hours p.i., with more enrichment at this timepoint shared between *Mtb*-only and co-infection, or all three infection conditions, with monocytes showing the greatest pathway enrichment, particularly for antigen presentation (II & III) and MHC-TLR7-TLR8 cluster, lysosomes in monocytes and both neutrophils and protein synthesis across all cell types, except neutrophils (GM-CSF) (Figure 3C, Supplementary Table 12).

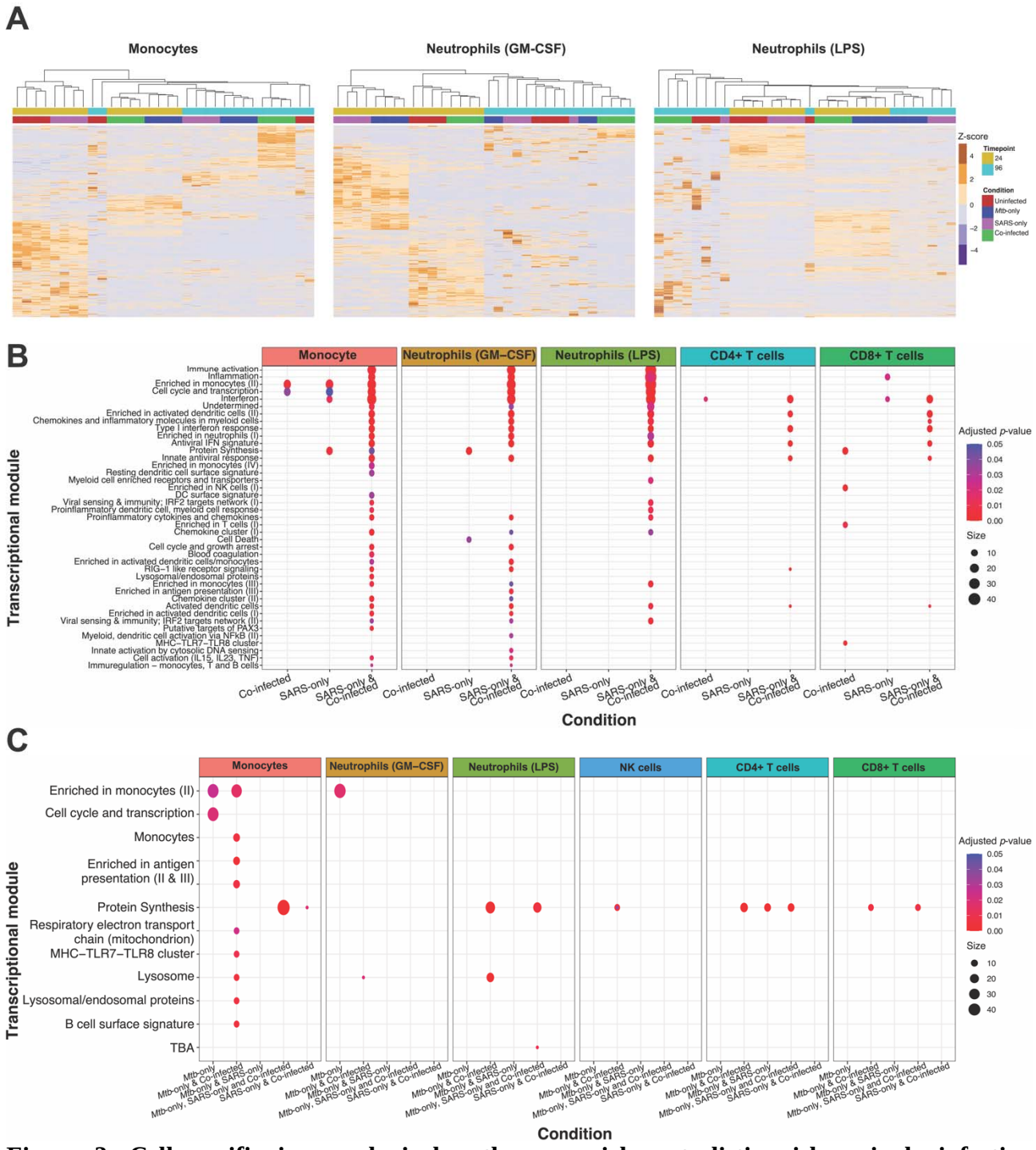

Figure 3. Cell-specific immunological pathway enrichment distinguishes single infection conditions and highlights synergistic activation in co-infected samples. Pseudobulk differential expression (DE) analysis was performed by splitting samples by annotated cell type and comparing these cell types from each infection condition with those of the uninfected samples at each timepoint, using donor IDs as biological replicates. The resultant signatures of significant genes were then used for hierarchical clustering across all samples, represented by the heatmaps in **A.**; the heat of the tiles correspond to the row z-score for a particular gene across all samples. Lists of significant genes for each cell type from each condition were subjected to blood transcriptional

451 module analysis to identify significantly enriched pathways associated with immune cells at **B.** 24
452 hours post-infection and **C.** 96 hours post-infection. False discovery rate-adjusted *p*-values are
453 representing by the shading of data points, while the size corresponds to the number of significant
454 genes implicated in that module.

Discussion

In the present study, we expand upon our previous work which identified overlapping transcriptional networks of circulating immune cells isolated from TB and COVID-19 patients [12] by delineating host immune cell gene expression programs in response to direct whole blood infection with *Mtb* and SARS-CoV-2 infection. Importantly, we directly compare responses induced by each pathogen alone to what occurs in the context of direct co-infection with both pathogens bringing us closer to an understanding of what is happening at a cellular level during TB/COVID-19 dual presentation. We define the host response pathways underlying differences between immune cell populations reacting to each infection condition across timepoints that appropriately capture innate and adaptive immune cell activity.

Despite the extensive use of bulk RNA-seq to study TB disease mechanisms in the blood of patients, there is but one study that defines host responses to *Mtb* by scRNA-seq in this compartment in which they sequenced PBMCs, excluding granulocytes [26]. There is substantial evidence that neutrophil gene expression is an important marker of TB progression [27-29], so any comprehensive characterisation of TB responses in human blood must include them. Despite their absence from a large number of blood scRNA-seq datasets, the COVID-19 scRNA-seq studies that did sequence neutrophils as part of whole blood found them to be an important cell type for distinguishing patients on the basis of disease severity [30, 31]. In our study, two neutrophil clusters emerged based on gene expression markers, neutrophils characterised by their response to GM-CSF/IFN-γ and those with enhanced response to LPS. The later were recovered in greater abundance in SARS-only and co-infected blood at 24 hours p.i, whilst only the GM-CSF neutrophils were enriched uniquely in SARS-only infection. Based on GO enrichment analyses, GM-CSF neutrophils appeared to have greater enrichment of IFN-γ and TNF regulation. These are both key cytokines implicated in *Mtb* control [32-34], so the fact they are not enriched to the same levels during co-infection, although they were more abundant than in *Mtb*-infection alone, suggests *Mtb* is interfering with their regulation by SARS-CoV-2. We previously identified IFN-γ and TNF signalling in the top 20 shared transcriptional pathways in blood of COVID-19 and TB patients and demonstrated *in vitro* that SARS-CoV-2 infected macrophages increase *TNF* and *IFNG* expression when pre-incubated in the inflammatory milieu of *Mtb* infected macrophages, correlating with increased SARS-CoV-2 transcript levels [12]. IFN-γ and TNF have been shown to act synergistically in a mouse model of COVID-19 by increasing inflammatory cell death through a process termed ‘PANoptosis’ [35]. Cell

death was also exclusively significantly enriched in these neutrophils in the SARS-only samples at 24 hours p.i.. Given the dramatic cell death observed at 96 hours p.i. in SARS-only and co-infected samples, with greater loss of cell recovery in SARS-only compared with co-infected, it is possible that early production of these cytokines from neutrophils may be one of the mechanisms underpinning this. A number of apoptosis regulation GO terms were significantly enriched in SARS-infected samples, with or without *Mtb* co-infection, at 24 hours p.i, including apoptotic cell clearance, extrinsic and intrinsic apoptotic signalling pathways, leukocyte and lymphocyte apoptotic processes and terms associated in the regulation of these pathways (Supplementary Table 9). At 96 hours p.i *Mtb*-only and co-infection shared enrichment of negative regulation of extrinsic apoptosis, which may underpin the increased recovered of cells from co-infected compared to SARS-only infected blood at 96 hours p.i. Caspase 8, the mediator of extrinsic apoptosis, has been identified as a critical factor in triggering inflammatory processes the lead to immunopathology in the lungs of COVID-19 patients [36]. Furthermore, caspase 8-dependent T cell apoptosis has been associated with T cell lymphopenia in severe COVID-19 patients, but this process could be prevented *ex vivo* with the use of pan-caspase inhibitors [37]. Given the critical role of T cells in *Mtb* control, early intervention to prevent T cell death from occurring in co-infected patients may be required to prevent TB disease progression.

Three neutrophil and monocyte cluster signatures were the greatest determinant of differences between the three infection conditions based on hierarchical clustering analyses. This ties in with evidence that innate immune cell gene expression, rather than lymphoid cells, marks the greatest divergence between COVID-19 severity across patients [30]. Monocytes were the cell type associated with the largest number of significantly enriched pathways, the majority of which were common to SARS-only and co-infected samples, specifically those related to immune activation, type I IFN responses and antigen presentation. Monocytes expressing high levels of HLA-DR and type I IFNs were identified in mild COVID-19 patients in the scRNA-seq study exploring myeloid cell dysregulation [30]. It has been shown that the activation status of monocytes are a correlate of COVID-19 prognosis, with inflammatory phenotypes associated with poorer outcomes [38]. Given that certain circulating monocytes have been identified in TB patients which correlate with disease progression, the induction of these activated, proinflammatory monocytes during co-infection may increase the likelihood of TB disease being advanced in co-infected individuals [39]. By 96 hours p.i. the greatest number of significantly enriched pathways was associated with and common to

517 monocytes from *Mtb*-only and co-infected samples and these pathways were mostly related to
518 lysosome and antigen presentation.

519 The most striking functional response induced by SARS-only/co-infection was the production of
520 IFNs, particularly those classified as type I (α and β). This observation runs counter to some early
521 human studies in which only low levels of type I IFN were measured in COVID-19 patients,
522 irrespective of disease severity [40], and subsequent studies that suggested little in the way of IFN
523 gene expression in peripheral blood from COVID-19 patients but an early transient wave of IFN-
524 stimulated genes (ISGs) [30, 41]. Mouse studies have indicated that the type I IFN response to
525 SARS-CoV-2 contributes more to immunopathology than viral control [42]. In TB, early expression
526 of ISGs in TB contacts has been linked to disease progression and worsened prognosis [29, 43-45].
527 Progression from earlier disease states to clinical TB is typically preceded by a wave of ISG
528 expression [29]. However, there is also evidence that type I IFN responses can be protective in TB
529 [46], and therefore it is likely that the influence of these IFNs on immune cell composition and
530 pathogenesis has a time-dependent effect over the course of TB disease [47]. It is plausible that
531 modulation of the type I IFN response in TB patients with a viral co-infection may alter the balance
532 in such a way as to promote TB disease progression. Over- or under-activation of type I IFN
533 responses is also known to contribute to host pathogenesis for viral infections [48], so it is equally
534 likely that an existing *Mtb* infection could negatively impact control of SARS-CoV-2 and promote
535 more severe disease manifestations. Our previous patient-level meta-analysis of COVID-19
536 signatures on TB datasets indicated that IFN gene signatures associated with COVID-19 severity
537 were highly significantly enriched in whole blood of TB progressors and their expression was the
538 strongest correlate of SARS-CoV-2 replication in macrophages [12], suggesting that the existence of
539 a strong TB IFN signature when SARS-CoV-2 co-infection occurs could be a key determinant of
540 poor outcomes for TB patients.

541 SARS-only samples had much lower proportions of CD4+ T cell, CD8+ T cell, B cell and NK cell
542 recovery at 24 hours. Longitudinal profiling of lymphocyte subsets in COVID-19 patients showed
543 that this occurs in patients shortly after symptom onset, when severe patients have lower proportions
544 of these cell types than those with mild infections, and they reach a nadir at 4–6 days post symptom
545 onset [49]. It has been reported that TB/COVID-19 co-infected patients have lower absolute
546 lymphocyte counts compared with COVID-19 patients [6]. This did not appear to be the case in our
547 study, although co-infected samples had lower proportions of lymphocytes than *Mtb*-only and

uninfected samples at 24 hours. We also observed a strong IFN signature in CD4+ and CD8+ T cells at 24 hours p.i. in the SARS-only and co-infected samples. A scRNA-seq study of peripheral blood responses in severe COVID-19 patients noted that the most commonly upregulated genes in these patients were ISGs based on their DE comparison with healthy controls [50]. At 96 hours p.i protein synthesis was commonly significantly enriched across all three infection conditions in CD4+ and CD8+ T cells. Enrichment of this pathway appeared to be mostly driven by expression of cathepsin genes, including *CTSB* and *CTSD*. These genes encode proteases, mainly found in lysosomes, which have been implicated in *Mtb* survival[51] and mediating SARS-CoV-2 binding [52].

The SARS-only samples had a greater proportion of B cells at 96 hours p.i.; several studies have noted an increase in the frequency of plasmablasts in severe COVID-19 patients [41, 53, 54]. However, this cell type was not captured at sufficient levels to perform any meaningful comparisons between groups to ascertain its function. NK cell proportions remained consistent in *Mtb*-only samples, as has been observed in TB patients compared even with TB-HIV co-infected patients [55, 56]. Only samples that were *Mtb*-infected had any significant pathway enrichment in NK cells, with enrichment for protein synthesis, including expression of *CTSD* as well as *PSAP* and *TPT1*, at the 96-hour timepoint. There is evidence that NK cell functionality plays a protective role by combating *Mtb* during HIV infection [57] that may also apply to other co-infections.

Our study is limited by the fact that we are studying the responses to pathogens in an artificial *ex vivo* infection model, so we do not recapitulate the natural course of infection, including the recruitment of new immune cells to replenish dying ones. Little is known about the mechanisms underlying human immune responses to the initial stages of *Mtb* infection as it is difficult to ascertain when exactly this occurs, while symptoms and diagnostics allow this to be better determined for SARS-CoV-2 infection. Our use of a reagent, TPCK trypsin, to cleave the SARS-CoV-2 spike glycoprotein and allow entry into host cells that do not express or have low levels of ACE2 receptor during initial infection also means that this model is not entirely representative of what occurs *in vivo*. This was done to increase the number of infected cells in our model, over the sort experimental timecourse. Human neutrophils have high levels of ACE2 expression and would be naturally infected and macrophages have been shown to be infected with SARS-CoV-2 in human lung autopsy sections and to be a site for viral replication [58]. We have also shown human macrophages to have increased susceptibility to SARS-CoV-2 infection in the absence of TPCK trypsin addition when incubated in *Mtb* inflammatory milieu [12]. Together this suggests there is the potential for ongoing SARS-CoV-2

infection of immune cells in our model, following TPCK trypsin removal. As not all cells will be infected, this approach allowed us to induce a reliable bystander response in cells that do not take up the virus that could then be compared between conditions. Despite the fact that SARS-CoV-2 transcripts undergo polyadenylation [59], we were unable to detect any viral transcripts in our count matrices. This may be due to insufficient sequencing depth or the capture efficiency of the scRNA-seq method used. Finally, simultaneous infection with *Mtb* and SARS-CoV-2 is unlikely to occur in most cases. With an established *Mtb* infection prior to SARS-CoV-2 infection more likely to reflect the vast majority of cases, as was observed in the TB/COVID Global Study Group report [4]. Nevertheless, in any co-infected individual there will always be new cells coming into an infection site, so that over time, irrespective of the first infecting pathogen, once both are present then any subsequent sequence of infection can occur.

In summary, we provide the first characterisation of human circulating immune cell gene expression changes resulting from direct *Mtb* and SARS-CoV-2 co-infection. We hope these data will provide a valuable resource for researchers and clinicians to gain insights to better characterise and identify points of potential therapeutic intervention or immunological exacerbation in TB/COVID-19 co-infected patients.

Conflict of Interest

The authors declare that the research was conducted in the absence of any commercial or financial relationships that could be construed as a potential conflict of interest.

Author Contributions

D.S. and A.K.C. conceived and designed the study. E.E. directed the COVID PROFILE clinical study, arranged blood sample collection, SARS-CoV-2 serotyping, and critically reviewed the manuscript. A.K.C. and E.E funded the study. T.K.P. generated SARS-CoV-2 virus stocks and critically reviewed the manuscript. D.S. generated *Mtb* stocks. D.S. performed blood infection experiments and processed samples for scRNA-seq. D.S. performed the data analysis. D.S. prepared the manuscript with editorial input and revisions from A.K.C. All authors approved the manuscript submission.

Funding

The COVID Profile study was supported by WHO Unity funds and WEHI Philanthropic funds. The funders had no role in study design, data collection and analysis. D.S. is supported by WEHI and NHMRC (2020750). A.K.C. is funded by WEHI, philanthropic donors, NHMRC (2020750) and the Australian Respiratory Council.

Acknowledgments

The authors thank Honeycomb Biotechnologies Inc. for allowing us to participate in their early access program, Maureen Forde for collecting blood samples from participants, Coussens Lab members for feedback, the WEHI PC3 Facility manager Kathryn Davidson for facility support, the WEHI Genomics R&D team, especially Rory Bowden, Daniela Zalcenstein, Daniel Brown and Ling Ling, for their input regarding experimental design and analysis, the Pellegrini Lab at WEHI for providing Vero cells and input into SARS-CoV-2 assays, and Stephen Wilcox of the WEHI Genomics Facility for performing Illumina sequencing of samples.

References

1. McQuaid, C.F., et al., *The impact of COVID-19 on TB: a review of the data.* Int J Tuberc Lung Dis, 2021. **25**(6): p. 436-446.
2. Migliori, G.B., et al., *Gauging the impact of the COVID-19 pandemic on tuberculosis services: a global study.* European Respiratory Journal, 2021. **58**(5): p. 2101786.
3. World Health Organization, *Global tuberculosis report 2022*. 2022.
4. The TB/COVID-19 Global Study Group, *Tuberculosis and COVID-19 co-infection: description of the global cohort.* European Respiratory Journal, 2022. **59**(3): p. 2102538.
5. Western Cape Department of Health in collaboration with the National Institute for Communicable Diseases South Africa, *Risk Factors for Coronavirus Disease 2019 (COVID-19) Death in a Population Cohort Study from the Western Cape Province, South Africa.* Clin Infect Dis, 2021. **73**(7): p. e2005-e2015.
6. Petrone, L., et al., *Coinfection of tuberculosis and COVID-19 limits the ability to in vitro respond to SARS-CoV-2.* Int J Infect Dis, 2021. **113 Suppl 1**: p. S82-s87.
7. Riou, C., et al., *Relationship of SARS-CoV-2–specific CD4 response to COVID-19 severity and impact of HIV-1 and tuberculosis coinfection.* The Journal of Clinical Investigation, 2021. **131**(12).
8. Rajamanickam, A., et al., *Latent tuberculosis co-infection is associated with heightened levels of humoral, cytokine and acute phase responses in seropositive SARS-CoV-2 infection.* Journal of Infection, 2021. **83**(3): p. 339-346.
9. Rajamanickam, A., et al., *Effect of SARS-CoV-2 seropositivity on antigen – specific cytokine and chemokine responses in latent tuberculosis.* Cytokine, 2022. **150**: p. 155785.

10. Hildebrand, R.E., et al., *Superinfection with SARS-CoV-2 Has Deleterious Effects on Mycobacterium bovis BCG Immunity and Promotes Dissemination of Mycobacterium tuberculosis.* Microbiology Spectrum, 2022. **10**(5): p. e03075-22.

11. Najafi-Fard, S., et al., *Characterization of the immune impairment of tuberculosis and COVID-19 coinfected patients.* International Journal of Infectious Diseases, 2023.

12. Sheerin, D., et al., *Immunopathogenic overlap between COVID-19 and tuberculosis identified from transcriptomic meta-analysis and human macrophage infection.* iScience, 2022. **25**(6): p. 104464.

13. Simpson, D.S., et al., *Interferon-γ primes macrophages for pathogen ligand-induced killing via a caspase-8 and mitochondrial cell death pathway.* Immunity, 2022. **55**(3): p. 423-441.e9.

14. Ramakrishnan, M.A., *Determination of 50% endpoint titer using a simple formula.* World J Virol, 2016. **5**(2): p. 85-6.

15. Emily, M.E., et al., *Cohort Profile: A longitudinal Victorian COVID-19 cohort (COVID PROFILE).* medRxiv, 2023: p. 2023.04.27.23289157.

16. Harris, P.A., et al., *Research electronic data capture (REDCap)--a metadata-driven methodology and workflow process for providing translational research informatics support.* J Biomed Inform, 2009. **42**(2): p. 377-81.

17. Harris, P.A., et al., *The REDCap consortium: Building an international community of software platform partners.* J Biomed Inform, 2019. **95**: p. 103208.

18. Huang, X. and Y. Huang, *Cellsnp-lite: an efficient tool for genotyping single cells.* Bioinformatics, 2021. **37**(23): p. 4569-4571.

19. Huang, Y., D.J. McCarthy, and O. Stegle, *Vireo: Bayesian demultiplexing of pooled single-cell RNA-seq data without genotype reference.* Genome Biology, 2019. **20**(1): p. 273.

20. Hafemeister, C. and R. Satija, *Normalization and variance stabilization of single-cell RNA-seq data using regularized negative binomial regression.* Genome Biol, 2019. **20**(1): p. 296.

21. Stuart, T., et al., *Comprehensive Integration of Single-Cell Data*. Cell, 2019. **177**(7): p. 1888-1902.e21.

22. Aran, D., et al., *Reference-based analysis of lung single-cell sequencing reveals a transitional profibrotic macrophage.* Nature Immunology, 2019. **20**(2): p. 163-172.

23. Wu, T., et al., *clusterProfiler 4.0: A universal enrichment tool for interpreting omics data.* The Innovation, 2021. **2**(3).

24. Love, M.I., W. Huber, and S. Anders, *Moderated estimation of fold change and dispersion for RNA-seq data with DESeq2.* Genome Biology, 2014. **15**(12): p. 550.

25. Zyla, J., et al., *Gene set enrichment for reproducible science: comparison of CERNO and eight other algorithms.* Bioinformatics, 2019. **35**(24): p. 5146-5154.

26. Cai, Y., et al., *Single-cell transcriptomics of blood reveals a natural killer cell subset depletion in tuberculosis.* EBioMedicine, 2020. **53**.

27. Berry, M.P.R., et al., *An interferon-inducible neutrophil-driven blood transcriptional signature in human tuberculosis.* Nature, 2010. **466**(7309): p. 973-977.

28. Bloom, C.I., et al., *Transcriptional blood signatures distinguish pulmonary tuberculosis, pulmonary sarcoidosis, pneumonias and lung cancers.* PLoS One, 2013. **8**(8): p. e70630.

29. Scriba, T.J., et al., *Sequential inflammatory processes define human progression from M. tuberculosis infection to tuberculosis disease.* PLoS Pathog, 2017. **13**(11): p. e1006687.

30. Schulte-Schrepping, J., et al., *Severe COVID-19 Is Marked by a Dysregulated Myeloid Cell Compartment.* Cell, 2020. **182**(6): p. 1419-1440.e23.

31. Silvin, A., et al., *Elevated Calprotectin and Abnormal Myeloid Cell Subsets Discriminate Severe from Mild COVID-19.* Cell, 2020. **182**(6): p. 1401-1418.e18.

32. Cooper, A.M., et al., *Disseminated tuberculosis in interferon gamma gene-disrupted mice.* J Exp Med, 1993. **178**(6): p. 2243-7.

33. Flynn, J.L., et al., *An essential role for interferon gamma in resistance to Mycobacterium tuberculosis infection.* J Exp Med, 1993. **178**(6): p. 2249-54.

34. Flynn, J.L., et al., *Tumor necrosis factor-alpha is required in the protective immune response against Mycobacterium tuberculosis in mice.* Immunity, 1995. **2**(6): p. 561-72.

35. Karki, R., et al., *Synergism of TNF-α and IFN-γ Triggers Inflammatory Cell Death, Tissue Damage, and Mortality in SARS-CoV-2 Infection and Cytokine Shock Syndromes.* Cell, 2021. **184**(1): p. 149-168.e17.

36. Li, S., et al., *SARS-CoV-2 triggers inflammatory responses and cell death through caspase-8 activation.* Signal Transduction and Targeted Therapy, 2020. **5**(1): p. 235.

37. André, S., et al., *T cell apoptosis characterizes severe Covid-19 disease.* Cell Death & Differentiation, 2022. **29**(8): p. 1486-1499.

38. Zhang, D., et al., *Frontline Science: COVID-19 infection induces readily detectable morphologic and inflammation-related phenotypic changes in peripheral blood monocytes.* J Leukoc Biol, 2021. **109**(1): p. 13-22.

39. Lastrucci, C., et al., *Tuberculosis is associated with expansion of a motile, permissive and immunomodulatory CD16+ monocyte population via the IL-10/STAT3 axis.* Cell Research, 2015. **25**(12): p. 1333-1351.

40. Hadjadj, J., et al., *Impaired type I interferon activity and inflammatory responses in severe COVID-19 patients.* Science, 2020. **369**(6504): p. 718.

41. Arunachalam, P.S., et al., *Systems biological assessment of immunity to mild versus severe COVID-19 infection in humans.* Science, 2020. **369**(6508): p. 1210-1220.

42. Israelow, B., et al., *Mouse model of SARS-CoV-2 reveals inflammatory role of type I interferon signaling.* J Exp Med, 2020. **217**(12).

43. Zak, D.E., et al., *A blood RNA signature for tuberculosis disease risk: a prospective cohort study.* Lancet, 2016. **387**(10035): p. 2312-2322.

44. Singhania, A., et al., *A modular transcriptional signature identifies phenotypic heterogeneity of human tuberculosis infection.* Nat Commun, 2018. **9**(1): p. 2308.

45. Esmail, H., et al., *Complement pathway gene activation and rising circulating immune complexes characterize early disease in HIV-associated tuberculosis.* Proceedings of the National Academy of Sciences, 2018. **115**(5): p. E964-E973.

46. Zhang, G., et al., *A proline deletion in IFNAR1 impairs IFN-signaling and underlies increased resistance to tuberculosis in humans.* Nature Communications, 2018. **9**(1): p. 85.

47. Desvignes, L., A.J. Wolf, and J.D. Ernst, *Dynamic roles of type I and type II IFNs in early infection with Mycobacterium tuberculosis.* J Immunol, 2012. **188**(12): p. 6205-15.

48. Mesev, E.V., R.A. LeDesma, and A. Ploss, *Decoding type I and III interferon signalling during viral infection.* Nat Microbiol, 2019. **4**(6): p. 914-924.

49. Liu, J., et al., *Longitudinal characteristics of lymphocyte responses and cytokine profiles in the peripheral blood of SARS-CoV-2 infected patients.* eBioMedicine, 2020. **55**.

50. Wilk, A.J., et al., *A single-cell atlas of the peripheral immune response in patients with severe COVID-19.* Nature Medicine, 2020. **26**(7): p. 1070-1076.

51. Pires, D., et al., *Role of Cathepsins in Mycobacterium tuberculosis Survival in Human Macrophages.* Sci Rep, 2016. **6**: p. 32247.

52. Zhang, Q., et al., *Molecular mechanism of interaction between SARS-CoV-2 and host cells and interventional therapy.* Signal Transduction and Targeted Therapy, 2021. **6**(1): p. 233.

53. Mathew, D., et al., *Deep immune profiling of COVID-19 patients reveals distinct immunotypes with therapeutic implications.* Science, 2020. **369**(6508).

54. Kuri-Cervantes, L., et al., *Comprehensive mapping of immune perturbations associated with severe COVID-19.* Sci Immunol, 2020. **5**(49).

55. Ardain, A., et al., *Group 3 innate lymphoid cells mediate early protective immunity against tuberculosis.* Nature, 2019. **570**(7762): p. 528-532.

56. Roy Chowdhury, R., et al., *A multi-cohort study of the immune factors associated with M. tuberculosis infection outcomes.* Nature, 2018. **560**(7720): p. 644-648.

57. Allen, M., et al., *Mechanisms of Control of Mycobacterium tuberculosis by NK Cells: Role of Glutathione*. Front Immunol, 2015. **6**: p. 508.

58. Sefik, E., et al., *Inflammasome activation in infected macrophages drives COVID-19 pathology.* Nature, 2022. **606**(7914): p. 585-593.

59. Chang, J.J., et al., *Long-Read RNA Sequencing Identifies Polyadenylation Elongation and Differential Transcript Usage of Host Transcripts During SARS-CoV-2 In Vitro Infection.* Front Immunol, 2022. **13**: p. 832223.

Data Availability Statement

The raw fastq files and processed transcript count matrices for this study can be found in the gene expression omnibus database under the accession number GSE232705. The scripts used to analyse these data have been uploaded to GitHub - https://github.com/sheerind-wehi/Mtb_SARS_co-infection

758